ACS APPLIED MATERIALS & INTERFACES

Research Article

www.acsami.org

Morphology and Photocatalytic Property of Hierarchical Polyimide/ZnO Fibers Prepared via a Direct Ion-exchange Process

Qianwei Ding, Yue-E Miao, and Tianxi Liu*

State Key Laboratory of Molecular Engineering of Polymers, Department of Macromolecular Science, Fudan University, Shanghai 200433, P. R. China

Supporting Information

ABSTRACT: A simple and efficient method has been developed for preparing hierarchical nanostructures of polyimide (PI)/ZnO fibers by combining electrospinning and direct ion-exchange process. Poly(amic acid) (PAA) nanofibers are first prepared by electrospinning, and then, the electrospun PAA fibers are immersed into $ZnCl_2$ solution. After a subsequent thermal treatment, imidization of PAA and formation of ZnO nanoparticles can be simultaneously achieved in one step to obtain PI/ZnO composite fibers. SEM images show that ZnO nanoparticles are densely and uniformly immobilized on the surface of electrospun PI fibers. Furthermore, the morphology of ZnO can be tuned from nanoplatelets to nanorods by changing the initial concentration of $ZnCl_2$ solution. Photocatalytic degradation tests show an efficient degradation ability of PI/ZnO composite membranes toward organic dyes. Meanwhile, the free-standing membrane is highly flexible, easy to handle, and easy to retrieve, which enables its use in water treatment. This simple and inexpensive approach can also be applied to fabricating other hierarchically nanostructured composites.

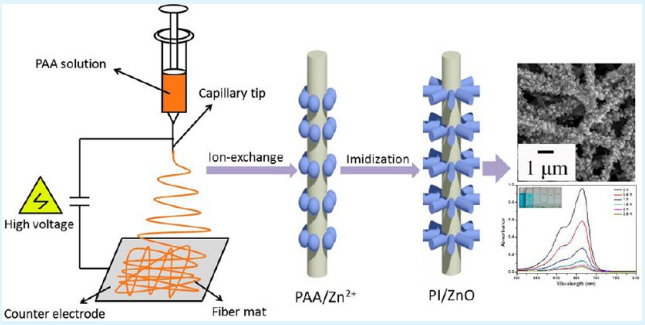

KEYWORDS: *electrospinning, ion-exchange, hierarchical structure, photocatalysis*

1. INTRODUCTION

In recent years, water pollution caused by organic and toxic pollutants has aroused great attention. Photocatalysis, as a "green" technique for the elimination of toxic chemicals in water, is of continuing interest. Various nanostructured semiconductor metal oxides, such as Fe_2O_3, TiO_2, and ZnO, have been developed as nanophotocatalysts for their ability to produce radicals and decompose most organic pollutants under UV irradiation or sunlight.[1] Among them, TiO_2 and ZnO have been recognized as the excellent materials for the degradation of environmental pollutants. ZnO is an *n*-type semiconductor with a direct bandgap of E_g = 3.35 eV. Compared to TiO_2, ZnO has a lower cost and a better efficiency in photocatalytic degradation for some organic dyes and has been extensively investigated and widely used recently.[2−5] Sakthivel et al. report that ZnO can absorb larger fraction of the solar spectrum and more light quanta than TiO_2 using sunlight as an energy source, showing a better photocatalytic efficiency in the degradation of acid brown 14.[6] Hariharan investigated the photodegradation of organic contaminants using the fluorescence emission characteristics of ZnO nanoparticles in aqueous solutions.[7] Yang et al. prepared the functionalized graphene sheets/ZnO nanocomposites via a thermal treatment method. This convenient and low-cost method made the composites excellent candidates in applications of catalysis and other areas.[8] Although the photocatalytic efficiency of ZnO nanoparticles is enhanced for its increased surface-to-volume ratios, their small dimension increases the tendency of nanoparticle aggregation and leads to difficulties in the separation from water. An effective strategy to solve these problems is to develop flexible fibrous membranes as substrate via electrospinning technique. The three-dimensional nanostructure of the fibrous membrane provides space for the growth of ZnO and improves the dispersity of ZnO nanoparticles. Hence, as the secondary component in the composite materials, ZnO exhibits superior performances in photocatalytic ability compared to ZnO nanoparticles.

Electrospinning has been used as an efficient technique to produce nanofibers with controllable diameter, large specific surface area and high porosity. The free-standing electrospun nanofiber membranes are promising in water treatment as they are easy to handle and retrieve.[9−12] Besides, the high porosity of the nanofiber membranes provides space for the growth of secondary nanostructures. Therefore, various hierarchical nanostructures have been obtained using electrospun fibrous membranes as matrix or template for applications in electronics, catalysis, and sensing applications.[13−16] Lee et al. immobilized TiO_2 nanoparticles on the surface of the electrospun poly(dimethylsiloxane-*b*-etherimide) (PSEI) nanofibers using a layer-by-layer (LbL) deposition approach. Although the colloidal TiO_2 nanoparticles showed a higher degradation rate

Received: March 15, 2013
Accepted: May 30, 2013
Published: May 30, 2013

   dx.doi.org/10.1021/am4009488 | ACS Appl. Mater. Interfaces 2013, 5, 5617−5622

constant initially, the multilayer-assembled TiO_2 nanofibers maintained the first-order kinetics for over 12 h and exhibited an 18.4% higher degradation of bisphenol A compared to colloidal TiO_2 nanoparticles.[17] Chang obtained ZnO/polyimide hybrid nanofibers by a combination of electrospinning technique and hydrothermal process, which showed high photocatalytic property for the degradation of rhodamine.[18] Fang et al. obtained polyethyleneimine (PEI)/polyvinyl alcohol (PVA) nanofibers by electrospinning, which were later treated with glutaraldehyde vapor to obtain cross-linked nanofibers. The abundant amine groups of PEI allowed for the binding of $AuCl^{4-}$ for subsequent formation and immobilization of Au nanoparticles.[19]

By selecting appropriate materials as nanofiber substrate and introducing specific functional materials onto nanofiber surfaces, multifunctional hierarchical nanofiber materials can be obtained. Polyimide (PI), as one kind of high-performance engineering polymers, has been widely used in many advanced technology fields due to its attractive properties such as high thermal stability, outstanding mechanical property and good chemical resistance.[20−23] Moreover, the carboxylic groups on the surface of poly(amic acid) (PAA), the precursor of polyimide, make it hydrophilic and provide cationic exchangeable sites to incorporate various metal ions. Several research groups have obtained metal oxide nanolayer on a flexible polyimide substrate via an ion exchange process. In their work, the PAA substrate was prepared by casting the precursor solution on glass. After remaining in slowly flowing air for 72 h, the PAA film was peeled from the glass and immerged into solutions to conduct ion-exchange reactions.[24−27] In our present work, hierarchical PI/ZnO fibers have been obtained by a combination of electrospinning and direct ion-exchange process. Through direct immersion of PAA nanofiber membranes into $ZnCl_2$ solution, followed by subsequent thermal treatment, imidization of PAA and formation of ZnO nanoparticles can be simultaneously achieved in one step, which is more convenient than other processes such as hydrothermal process in obtaining hierarchical nanostructures. Moreover, the morphology of ZnO grown on the electrospun nanofibers can be tuned from nanoplatelets to nanorods by simply changing the concentration of $ZnCl_2$ solution. The obtained membranes with hierarchical structures provide an open three-dimensional network with high active surface area, thus facilitating the entrance of water and adsorption of pollutants in water purification. Therefore, an efficient degradation ability of PI/ZnO composite membranes toward organic dyes has been obtained, which may be applied to water decontamination. Compared to the hydrothermal process, this simple and inexpensive method is also energy-saving.

2. EXPERIMENTAL SECTION

Materials. Pyromellitic dianhydride (PMDA), 4,4′-oxidianiline (ODA), and *N*,*N*-dimethylacetamide (DMAc) were commercially purchased from China Medicine, Co. All other reagents were purchased from Aladdin Chemical Reagent, Co., Ltd. and used as received.

Preparation of Electrospun Poly(Amic Acid) (PAA) Nanofiber Membranes. PAA, the precursor of polyimide, was synthesized by the polycondensation of PMDA and ODA with an equivalent molar ratio in DMAc at 0 °C. After reaction for 5 h, a yellow viscous solution with a 20 wt % solid content was obtained. Then, the solid content of PAA solutions was diluted to 13 wt % for electrospinning. The electrospinning solution was loaded into a 5 mL syringe with a spinneret which had a diameter of 0.5 mm. A voltage of 20 kV was attached to the spinneret. The electrospun fibers were collected onto the rotating aluminum collector with a diameter of 0.30 m and a width of 8 mm, which was placed 15 cm away from the needle. The membrane was overnight dried at 60 °C in vacuum for 2 h to remove the residual solvent.

One-Step Imidization of PAA and Formation of ZnO Nanoparticles on the Membranes. The prepared PAA nanofiber membranes were first immersed into $ZnCl_2$ solutions with different concentrations (0.2, 0.5, 1, and 2 M) for 2 h, respectively. After that, the membranes were rinsed for three times with deionized water to remove the residual $ZnCl_2$ solution. Then, the thermal imidization process was completed by the following program: heating up to 100, 200, and 300 °C at a heating rate of 3 °C/min, keeping an annealing at each temperature for 0.5 h. Thus, PI/ZnO nanofiber membranes were obtained in a whole preparation procedure as shown in Figure 1. Here, the PAA membranes immersed into different $ZnCl_2$ solutions (0.2 M, 0.5 M, 1 M, 2 M) are referred as 0.2 M PI/ZnO, 0.5 M PI/ZnO, 1 M PI/ZnO, and 2 M PI/ZnO, respectively.

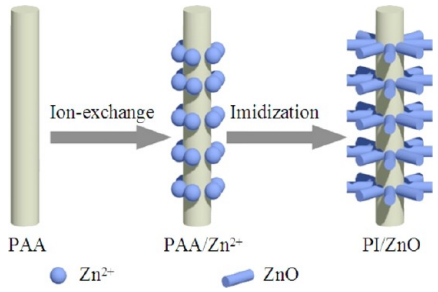

Figure 1. Schematic of the preparation of hierarchical PI/ZnO nanofibers.

Characterizations. The surface morphology of the samples was observed under a scanning electron microscope (SEM, Tescan) at an acceleration voltage of 20 kV. Phase structure of the samples was examined by X-ray diffraction (XRD) with Cu Kα radiation (λ = 0.1542 nm). Thermogravimetric analysis (TGA) was performed in air from 100 to 800 °C at a heating rate of 20 °C/min.[28−30] The photocatalytic reaction was carried out with a low pressure mercury lamp applied as the UV light source and methylene blue (MB) as the dye pollutant. Five mg membranes were immersed into the MB solution (5 mg L^{-1}) and stored in the dark for 0.5 h to ensure the adsorption/desorption balance of MB. Then, the degradation of MB was monitored by UV spectrum at scheduled time intervals.

3. RESULTS AND DISCUSSION

PAA was chosen as the electrospun matrix because of its good spinnability and hydrophilicity. By changing the content of DMAc, the optimized solid content of PAA solution was fixed at 13 wt % for an appropriate viscosity. Figure 2A and 2B show

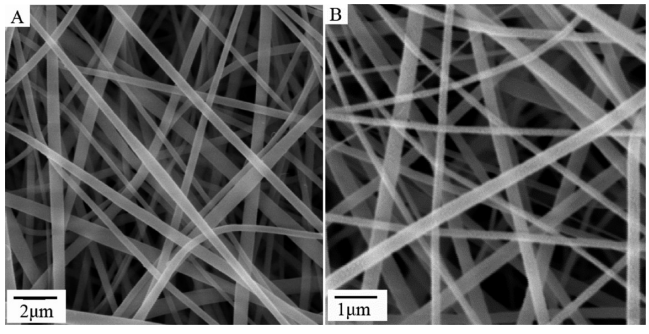

Figure 2. SEM images at low (A) and high (B) magnifications of PAA (13 wt %) nanofibers.

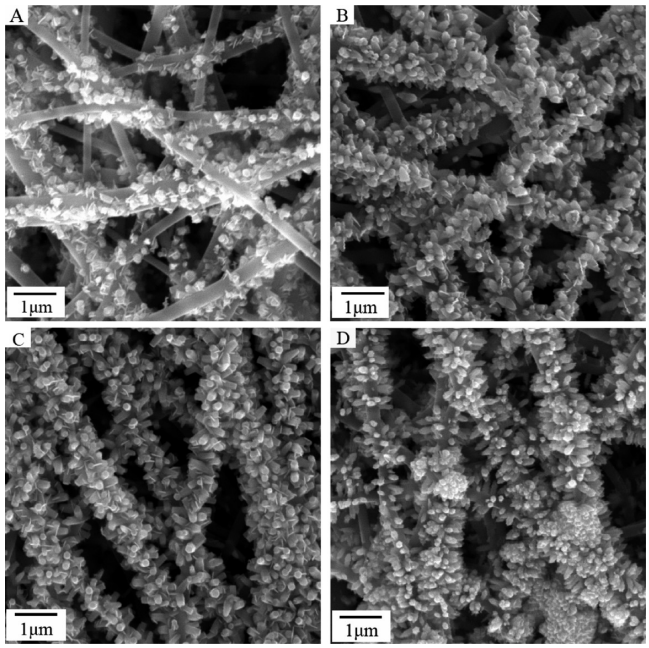

Figure 3. SEM images of PI/ZnO nanofibers obtained by ion-exchange in $ZnCl_2$ solutions: (A) 0.2 M PI/ZnO, (B) 0.5 M PI/ZnO, (C) 1 M PI/ZnO, and (D) 2 M PI/ZnO.

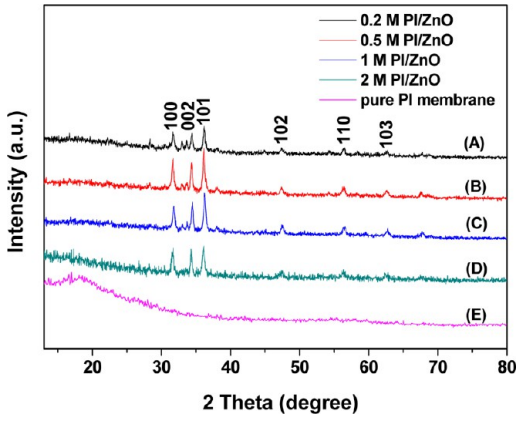

Figure 4. XRD patterns of the samples prepared by the same method with different conditions: (A) 0.2 M PI/ZnO, (B) 0.5 M PI/ZnO, (C) 1 M PI/ZnO, (D) 2 M PI/ZnO, and (E) neat PI membrane.

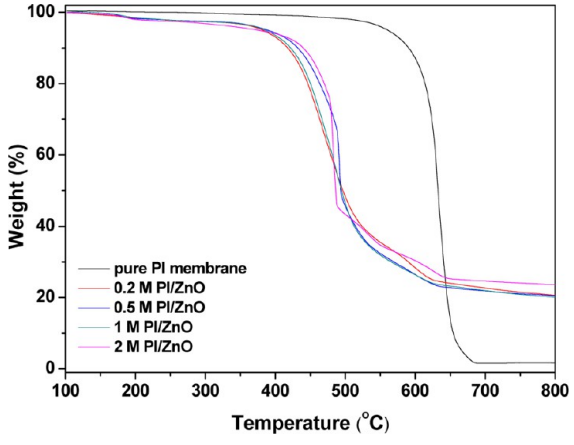

Figure 5. TGA curves of neat PI membrane and PI/ZnO nanofiber membranes obtained in different $ZnCl_2$ solutions.

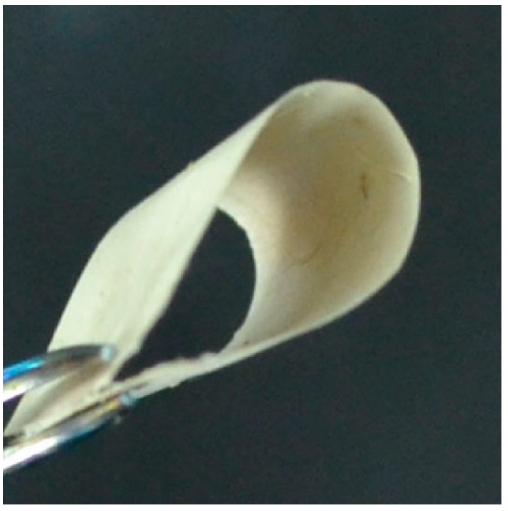

Figure 6. Digital photo of the self-standing PI/ZnO nanofiber membrane.

the SEM images of PAA nanofibers at low and high magnifications, respectively. The fibers have a diameter of about 150−300 nm and a smooth surface without obvious beads or breakages, which can be beneficial for the following ion-exchange process. As seen in Supporting Information Figure S1, the smooth surface of the electrospun fibers can be observed clearly. In addition, the randomly oriented nanofibers exhibit highly porous structures, which can provide space for subsequent growth of nanoparticles and facilitate the permeation of water.

To thoroughly investigate the effect of the concentration of $ZnCl_2$ solution on the morphology of ZnO, a series of PI/ZnO nanofiber membranes were obtained through the direct ion-exchange process. The surface morphology of the nanofibers is presented in Figure 3. From the SEM images it can be observed that the ZnO nanoparticles are evenly distributed on the surface of PI nanofibers after the thermal imidization process. Moreover, the morphology of ZnO is clearly observed to be from nanoplatelets to nanorods as the concentration of $ZnCl_2$ solution increases. For the 0.2 M PI/ZnO composite membrane (Figure 3A), there are small ZnO nanoplatelets sparsely distributed on the nanofiber surface. Further increasing the concentration of $ZnCl_2$ to 0.5 M (Figure 3B), well-defined ZnO nanoplatelets mixed with a few nanorods are radially grown on the electrospun PI nanofibers with a high coverage density, almost over the entire nanofibers. The morphology of 1 M PI/ZnO is shown in Figure 3C. It can be seen that well-defined ZnO nanorods with hexagonal structures are gradually grown densely and uniformly on the PI nanofibers. The nanorods show a diameter of about 100 nm and a length of 300 nm, which can be observed in Supporting Information Figure S2 (A) at a higher magnification. When the $ZnCl_2$ concentration is increased to 2 M (Figure 3D), agglomerated ZnO nanorods are observed on the surface of PI nanofibers. The morphology of the nanostructures plays a vital factor in the photocatalytic process since the photocatalytic degradation process occurs mainly at the interface of the catalyst and the pollutant. From Figure 3, it can be deduced that higher concentration of the $ZnCl_2$ solution improves the interaction between the fiber and Zn^{2+}, resulting in higher content of Zn^{2+} loaded on the nanofibers. However, the excessive concentration of $ZnCl_2$ solutions may lead to aggregation of ZnO nano-

dx.doi.org/10.1021/am4009488 | ACS Appl. Mater. Interfaces 2013, 5, 5617−5622

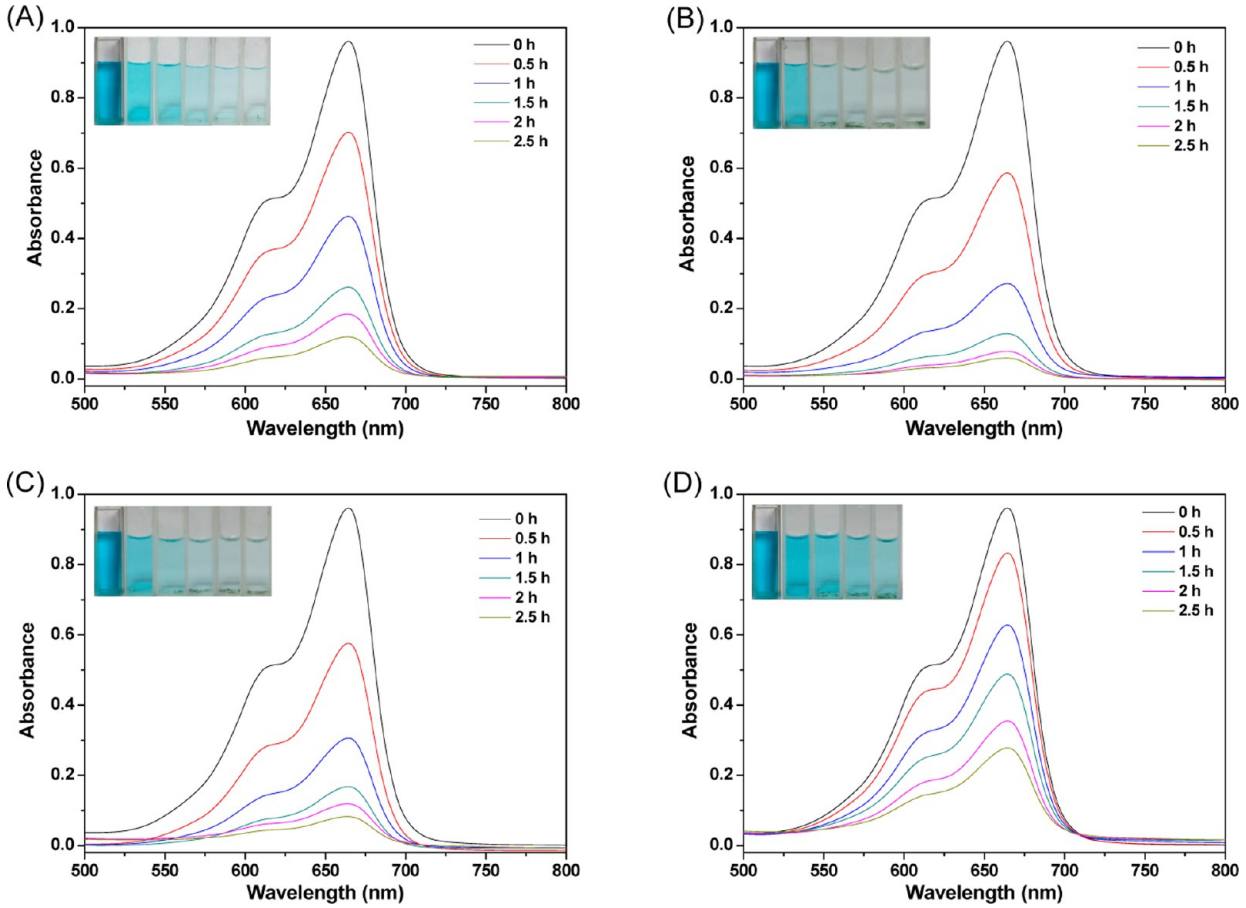

Figure 7. Time dependent UV−vis absorbance of the MB solution after photodegradation by different membranes: (A) 0.2 M PI/ZnO, (B) 0.5 M PI/ZnO, (C) 1 M PI/ZnO, and (D) 2 M PI/ZnO. The insets are the digital photos showing the whole photocatalytic process.

particles and thus affect the photocatalytic property. Therefore, a hierarchical three-dimensional network of PI/ZnO fibers is constructed by the combination of electrospinning and direct ion-exchange process. This unique nanostructure is expected to improve the photocatalytic degradation efficiency of the prepared PI/ZnO composite fibers.

The structure of ZnO nanoparticles on the PI nanofiber surface can be confirmed through XRD analysis. The corresponding XRD patterns of the samples are shown in Figure 4. Compared to the XRD curve of the pristine PI membrane in Figure 4E, the additional diffraction peaks with 2θ values in Figure 4A−4D can be perfectly indexed as (002), (100), (101), (102), (103), and (110) crystal planes of the hexagonal wurtzite ZnO (JCPDS 36-1451). Therefore, the XRD results also indicate the formation of ZnO on the surface of PI nanofibers after thermal treatment.

TGA was conducted to further analyze the content of ZnO on the PI nanofibers, as shown in Figure 5. From the TGA curve of the neat PI nanofiber membrane, it can be observed that PI is almost completely degraded at 800 °C. Thus, the loading amount of ZnO in all the PI/ZnO composite nanofiber membranes is calculated to be approximately 20 wt %. The reason why the amount of ZnO obtained by TGA seems to be almost the same in spite of an increase of the ZnO incorporation on the fiber surface by SEM is probably related to the thickness of the membrane. With the increase of the concentration of $ZnCl_2$ solution, the dense growth of ZnO on the surface of membrane will make it difficult for Zn^{2+} to enter the inside region of the membrane. Therefore, the loading amount of ZnO nanoparticles in the inside of the membranes may be slightly decreased with increasing the concentration of $ZnCl_2$ solution. Thus, the loadings of ZnO in all the PI/ZnO composite nanofiber membranes are almost the same from the TGA results. In addition, as discussed above, the concentration of $ZnCl_2$ solution mainly affects the morphology of ZnO. Therefore, the SEM images (qualitatively) do not have a direct or an exact (quantitative) relationship with the loading amount of ZnO in composite membranes. In addition, the PI/ZnO composite nanofiber membranes underwent a significant weight loss at a much lower onset temperature of degradation (T_{onset}) compared to that of the pristine PI membrane. The decrease of the thermal stability is probably caused by the oxidative degradation of PI catalyzed by the newly born ZnO nanoparticles during the thermal treatment. Although the thermal stability of the composite membranes is not as good as the pristine PI membrane, they still maintain excellent thermal stability with T_{onset} over 400 °C. Moreover, although the composite membranes show color change from light yellow to gray after imidization, they still exhibit good flexibility with no crack after several times of bending as shown in Figure 6, which may be due to the small size of the fibers.[31] Therefore, the high flexibility, retrievability and three-dimensional nanostructures of PI/ZnO composite membranes make them superior over ZnO nanoparticles in water purification.

The photocatalytic property of the composite membranes prepared from $ZnCl_2$ solutions with different concentrations

dx.doi.org/10.1021/am4009488 | ACS Appl. Mater. Interfaces 2013, 5, 5617−5622

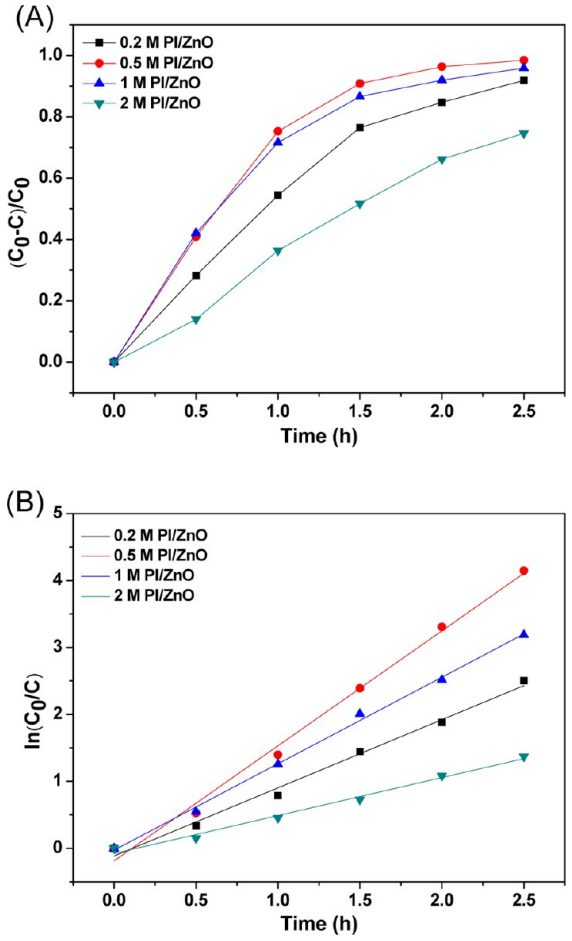

Figure 8. Degradation curves (A) and the $\ln(C_0/C)$ versus time curves (B) obtained in the presence of different membranes.

was evaluated with MB as an organic pollutant. The time dependent UV absorption spectra of MB are shown in Figure 7, which show the photocatalytic activities of 0.2 M PI/ZnO, 0.5 M PI/ZnO, 1 M PI/ZnO, and 2 M PI/ZnO composite membranes toward MB, respectively. The change in absorption spectra of MB aqueous solution shows the change of its concentration. The obvious decrease in the absorption peaks of the UV absorption spectra of MB indicates an efficient adsorption of MB on the membranes. Figure 7B shows a more obvious decrease in the absorption peaks than the others, indicating a more efficient degradation efficiency of the 0.5 M PI/ZnO composite membrane toward MB. The insets of Figure 7 clearly exhibit the color change of MB solutions during the whole degradation process.

The photocatalytic performance is illustrated quantitatively by the peak values at 662 nm of the absorption spectra of MB (Figure 8A). The degradation rate (D%) can be calculated as the following expression:

$$D\% = \frac{C_0 - C}{C_0} 100\% \quad (1)$$

where C_0 is the initial concentration of MB, and the C is the final concentration at time t. From the degradation curves, it can be seen that the degradation rate of 0.2 M PI/ZnO, 0.5 M PI/ZnO, 1 M PI/ZnO and 2 M PI/ZnO composite membranes toward MB after 2.5 h is about 92%, 98%, 96%, 75%, respectively. Moreover, the 0.5 M PI/ZnO composite membrane performs an optimum catalytic activity while the photocatalytic performance of the 2 M PI/ZnO membrane is not as excellent as the others in the whole degradation process. In addition, the contact surface area between the catalyst and the pollutants, which is determined by the morphology of the catalyst, is a vital factor in the photocatalytic process since the catalytic reaction mainly occurs at their interface.[32] The 0.5 M PI/ZnO composite membrane shows a high density of ZnO nanoplatelets and provides a large contact surface area, thus resulting in an excellent photocatalytic activity. A less efficient degradation shown by the 2 M PI/ZnO sample may be caused by the aggregation of ZnO particles on the surface of PI nanofibers, which results in a smaller active contact area between the photocatalyst and the pollutant, compared to the other composite membranes.

The kinetic simulation curves of the photocatalytic degradation of MB over the obtained composite membranes are shown in Figure 8B. The photodegradation process of the hierarchical nanofibers can be considered as a pseudo-first-order reaction with the following kinetic equation:

$$\ln(C_0/C) = kt \quad (2)$$

where k is the degradation rate constant. The degradation rate constants of 0.2 M PI/ZnO, 0.5 M PI/ZnO, 1 M PI/ZnO, and 2 M PI/ZnO composite membranes are about 1.0, 1.7, 1.3, and 0.6 h^{-1}, respectively. The degradation rate constant of 0.5 M PI/ZnO is about three times of the 2 M PI/ZnO sample, showing higher photocatalytic efficiency. Moreover, the degradation rate constant of the 0.5 M PI/ZnO sample is much higher than that of ZnO powder and comparable to those of composites containing ZnO component.[16,33,34]As a result, the degradation efficiency increases with increasing the concentration of $ZnCl_2$ solution, and then the efficiency decreases when the concentration is increased to 2 M. The results indicate that the morphology of ZnO grown on the nanofibers probably has an effect on the photocatalytic efficiency. As seen in Figure 3, the 0.5 M PI/ZnO sample possesses more ZnO nanoplatelets compared to the other samples, resulting in a larger contact surface area and higher photocatalytic efficiency. In addition, the nanoplatelets grown on the 0.5 M PI/ZnO sample can be observed clearly in Supporting Information Figure S2 (B) at a higher magnification. Moreover, dense and uniform distribution of ZnO on the surface of PI nanofibers will increase the total contact surface area, namely the number of active sites available for catalytic reaction between ZnO and the pollutants. Finally, the decrease in the photocatalytic efficiency when the concentration of $ZnCl_2$ solution is increased to 2 M seems to be due to the reduced light penetration, the increased light scattering, and the loss in surface area occasioned by aggregation of ZnO nanoparticles on the surface of PI nanofibers.

4. CONCLUSIONS

A series of polyimide/ZnO nanofiber membranes obtained from different concentrations of $ZnCl_2$ solutions have been fabricated by combining electrospinning and direct ion-exchange process. Processing simplicity makes the direct ion-exchange process more convenient than the hydrothermal process for preparing the hierarchical nanostructures. The porous three-dimensional nanostructure of the composite membranes provides large active surface area for photocatalysis, and permits the permeation of polluted water. Besides, the morphology of ZnO can be tuned from nanoplatelets to

dx.doi.org/10.1021/am4009488 | ACS Appl. Mater. Interfaces 2013, 5, 5617−5622

nanorods by adjusting the concentration of $ZnCl_2$ solution, and the ZnO morphology significantly affects the photocatalytic activity. The 0.5 M PI/ZnO composite membrane is proved to be optimum and exhibits outstanding photocatalytic degradation property. The PI/ZnO composite membranes prepared are highly flexible and easy to handle, enabling their uses in water remediation and other applications.

■ ASSOCIATED CONTENT

Supporting Information

TEM image of electrospun PAA nanofibers, SEM images at high magnifications for PI/ZnO nanofibers obtained by ion-exchange in $ZnCl_2$ solutions: (A) 1.0 M PI/ZnO and (B) 0.5 M PI/ZnO. This material is available free of charge via the Internet at http://pubs.acs.org.

■ AUTHOR INFORMATION

Corresponding Author

*Tel: 86-21-55664197. Fax: 86-21-65640293. E-mail: txliu@fudan.edu.cn.

Notes

The authors declare no competing financial interest.

■ ACKNOWLEDGMENTS

The authors are grateful for the financial support from the National Natural Science Foundation of China (51125011).

■ REFERENCES

(1) Hoffmann, M. R.; Martin, S. T.; Choi, W.; Bahnemann, D. W. *Chem. Rev.* **1995**, *95*, 69−96.
(2) Akyol, A.; Yatmaz, H. C.; Bayramoglu, M. *Appl. Catal., B* **2004**, *54*, 19−24.
(3) Chakrabarti, S.; Dutta, B. K. *J. Hazard. Mater.* **2004**, *112*, 269−278.
(4) Li, B. J.; Cao, H. Q. *J. Mater. Chem.* **2011**, *21*, 3346−3349.
(5) Wang, Y.; Li, X.; Wang, N.; Quan, X.; Chen, Y. *Sep. Purif. Technol.* **2008**, *62*, 727−732.
(6) Sakthivel, S.; Neppolian, B.; Shankar, M. V.; Arabindoo, B.; Palanichamy, M.; Murugesan, V. *Sol. Energy Mater. Sol. Cells* **2003**, *77*, 65−82.
(7) Hariharan, C. *Appl. Catal., A* **2006**, *304*, 55−61.
(8) Yang, Y.; Ren, L. L.; Zhang, C.; Huang, S.; Liu, T. X. *ACS Appl. Mater. Interfaces* **2011**, *3*, 2779−2785.
(9) Chronakis, I. S. *J. Mater. Process. Technol.* **2005**, *167*, 283−293.
(10) Reneker, D. H.; Yarin, A. L. *Polymer* **2008**, *49*, 2387−2425.
(11) Huang, Z. M.; Zhang, Y. Z.; Kotaki, M.; Ramakrishna, S. *Compos. Sci. Technol.* **2003**, *63*, 2223−2253.
(12) Reneker, D. H.; Chun, I. *Nanotechnology* **1996**, *7*, 216−223.
(13) Sun, C. H.; Wang, N. X.; Zhou, S. Y.; Hu, X. J.; Chen, P. *Chem. Commun.* **2008**, 3293−3295.
(14) Mu, J. B.; Shao, C. L.; Guo, Z. C.; Zhang, Z. Y.; Zhang, M. Y.; Zhang, P.; Chen, B.; Liu, Y. C. *ACS Appl. Mater. Interfaces* **2011**, *3*, 590−596.
(15) Zhang, Z. Y.; Shao, C. L.; Li, X. H.; Zhang, L.; Xue, H. M.; Wang, C. H.; Liu, Y. C. *J. Phys. Chem. C* **2010**, *114*, 7920−7925.
(16) Wang, R. Y.; Guo, J.; Chen, D.; Miao, Y. E.; Pan, J. S.; Tjiu, W. W.; Liu, T. X. *J. Mater. Chem.* **2011**, *21*, 19375−19380.
(17) Lee, J. A.; Nam, Y. S.; Rutledge, G. C.; Hammond, P. T. *Adv. Funct. Mater.* **2010**, *20*, 2424−2429.
(18) Chang, Z. J. *Chem. Commun.* **2011**, *47*, 4427−4429.
(19) Fang, X.; Ma, H.; Xiao, S.; Shen, M.; Guo, R.; Cao, X.; Shi, X. *J. Mater. Chem.* **2011**, *21*, 4493−4501.
(20) Chung, G. S.; Jo, S. M.; Kim, B. C. *J. Appl. Polym. Sci.* **2005**, *97*, 165−170.
(21) Chen, D.; Liu, T. X.; Zhou, X. P.; Tjiu, W. C.; Hou, H. Q. *J. Phys. Chem. B* **2009**, *113*, 9741−9748.
(22) Arlen, M. J.; Wang, D.; Jacobs, J. D.; Justice, R.; Trionfi, A.; Hsu, J. W. P.; Schaffer, D.; Tan, L. S.; Vaia, R. A. *Macromolecules* **2008**, *41*, 8053−8062.
(23) Cheng, C. Y.; Chen, J.; Chen, F.; Hu, P.; Wu, X. F.; Reneker, D. H.; Hou, H. Q. *J. Appl. Polym. Sci.* **2010**, *116*, 1581−1586.
(24) Akamatsu, K.; Ikeda, S.; Nawafune, H.; Deki, S. *Chem. Mater.* **2003**, *15*, 2488−2491.
(25) Ikeda, S.; Akamatsu, K.; Nawafune, H.; Nishino, T.; Deki, S. *J. Phys. Chem. B* **2004**, *108*, 15599−15607.
(26) Mu, S. X.; Wu, D. Z.; Wang, Y.; Wu, Z. P.; Yang, X. P.; Yang, W. T. *ACS Appl. Mater. Interfaces* **2010**, *2*, 111−118.
(27) Cui, G. H.; Wu, D. Z.; Qi, S. L.; Jin, S.; Wu, Z. P.; Jin, R. G. *ACS Appl. Mater. Interfaces* **2011**, *3*, 789−794.
(28) Xu, Z.; Gao, C. *Macromolecules* **2010**, *43*, 6716−6723.
(29) Zhang, P.; Chen, Y.; Li, G. Q.; Luo, L. B.; Pang, Y. W.; Wang, X.; Peng, C. R.; Liu, X. Y. *Polym. Advan. Technol.* **2012**, *23*, 1362−1368.
(30) Guo, H. Q.; Meador, M.; McCorkle, L. *ACS Appl. Mater. Interfaces* **2012**, *4*, 5422−5429.
(31) Guo, M.; Ding, B.; Li, X.; Wang, X.; Yu, J.; Wang, M. *J. Phys. Chem. C* **2010**, *114*, 916−921.
(32) Li, D.; Haneda, H. *Chemosphere* **2003**, *51*, 129−137.
(33) Chauhan, R.; Kumar, A.; Chaudhary, R. P. *J. Sol−Gel Sci. Technol.* **2012**, *63*, 546−553.
(34) Eskizeybek, V.; Sari, F.; Gulce, H. *Appl. Catal., B* **2012**, *119*, 197−206.